

# Photoinitiated crosslinked degradable copolymer networks for tissue engineering applications

Kelly A. Davis<sup>a,b</sup>, Jason A. Burdick<sup>b</sup>, Kristi S. Anseth<sup>a,b,\*</sup>

<sup>a</sup>Howard Hughes Medical Institute, University of Colorado, Campus Box 424, Boulder, CO 80309, USA

<sup>b</sup>Department of Chemical Engineering, University of Colorado, Campus Box 424, Boulder, CO 80309, USA

Received 3 August 2002; accepted 13 November 2002

## Abstract

Diethylene glycol was used to initiate the ring opening polymerization of D,L-lactide and  $\epsilon$ -caprolactone, as well as combinations of the two monomers. Esterification of the oligomer end groups with methacryloyl chloride led to divinyl terminated macromers that were reacted via photoinitiated polymerizations to produce crosslinked networks. The lactic and/or caproic acid repeat units can be hydrolyzed under physiological conditions, leading to degradable networks that may be useful for tissue engineering applications. Specifically, methacryloyl terminated poly(lactic acid-co-caproic acid) diethylene glycol based oligomers were prepared and characterized by <sup>1</sup>H NMR. The number of ester linkages was kept constant while the ratio of lactic:caproic acid segments was varied. These macromers were then photopolymerized at 450 nm using a visible light initiating system to produce crosslinked degradable networks. The kinetics of the polymerizations were followed by DSC, and the dynamic mechanical behavior was monitored as a function of temperature to obtain the  $T_g$  for each network composition. 1 mm thick disks were subjected to hydrolytic degradation in an aqueous phosphate buffer solution at a pH = 7.4 and 37°C. The changes in the compressive modulus, as well as the % mass loss as a function of time, were recorded. Cellular compatibility was determined by seeding primary rat calvarial osteoblast cells onto the disks and characterizing the cell morphology using scanning electron microscopy.

© 2003 Elsevier Science Ltd. All rights reserved.

**Keywords:** Crosslinked degradable networks; Visible light; Mechanical properties; Cellular compatibility;  $\alpha$ -hydroxy acid copolymers

## 1. Introduction

Recent trends in the development of in situ forming biomaterials have focused on preparing multifunctional monomers that contain reactive groups to form cross-linked scaffolds. These materials are potentially useful for a variety of tissue engineering applications, including bone fixation [1–8], cartilage repair [9–12], and delivery of therapeutic agents [13–20]. There are several advantages to in situ forming materials compared to prefabricated ones. Generally, the precursors are readily injected or moldable, allow for facile filling of oddly shaped defects, and enable homogeneous encapsulation of cells and/or therapeutic molecules. For many tissue engineering applications, enhanced adhesion and integration of the biomaterial with the existing tissue may also occur since curing takes place in situ rather than

pre-implantation. Less invasive surgical methods may also be possible when using more liquid like materials that can be injected and polymerized arthroscopically or transdermally [21,22].

In designing in situ forming biomaterials, photoinitiated polymerizations offer many advantages and have become a mainstay in the biomaterials arena. Multi-methacrylate monomers have been photopolymerized to form dental fillings for many years [23], and research into the cytotoxicity of various photoinitiators has shown that several are biocompatible [24]. This has led to the use of photopolymerizations for cell encapsulation within biomaterials [12,25,26], which has important implications for tissue regeneration, particularly with regard to the uniformity of tissue growth in materials where cell migration is the main method of infiltration.

Photopolymerizations also offer improved temporal control of the initiation process when compared to methods such as redox initiation systems, as they are controlled by the presence of light. For example, this feature might be beneficial when designing a

\*Corresponding author. Tel.: +1-303-492-3147; fax: +1-303-492-4341.

E-mail address: [kristi.anseth@colorado.edu](mailto:kristi.anseth@colorado.edu) (K.S. Anseth).

contourable implant. The system would be partially cured prior to implantation and fully cured post-implantation, providing more time for manipulation of the material for maximum efficiency. Additionally, temporal control can be utilized to minimize the temperature rise during the polymerization, which can prevent extensive necrosis of tissues at the implantation site. The polymerizations are complete in a minimal amount of time, making them ideal for a surgical setting. The rate can be adjusted by altering the polymerization conditions, including the choice and concentration of the photoinitiator, the concentration of reactive double bonds in the formulation, the wavelength of the light source (UV or visible), as well as the light intensity. Enhanced spatial control is another advantage of using photopolymerizations. Patterned surfaces may be necessary when highly organized tissue development is desired, as is the case for nerve regeneration. All of these components combine to make photoinitiated polymerizations attractive for in situ biomaterials formation.

Since photopolymerizations generally take place via a chain growth process, degradation is often restricted to the network crosslinks, which allows for using alternative chemistries to incorporate degradable linkages into these crosslinks. This aspect of designing photocrosslinkable and degradable biomaterials has garnered substantial interest [27]. Whether degradation occurs through the hydrolysis of labile bonds [13,28] or via enzymatic attack [14,29], photopolymerized degradable scaffolds have been investigated for numerous applications, including controlled release [27], bone tissue engineering [30], and wound healing [17], among others. Photopolymerization has been used to prepare degradable hydrogels based on poly(ethylene glycol)/ $\alpha$ -hydroxy acid copolymers [28,31,32], as well as highly cross-linked hydrophobic scaffolds based on poly(anhydrides) [4,33] or diethylene glycol/ $\alpha$ -hydroxy acid copolymers [34].

Perhaps the most beneficial aspect of using cross-linked degradable scaffolds for tissue engineering applications is the ability to tailor the network properties through both the chemical make-up and structure of the precursor macromolecules. For example, the degradation rate can be controlled not only through the number of degradable linkages present on the cross-linking molecule, but by its molecular weight as well, which directly influences the crosslinking density and, in turn the mechanical properties. In a simplified manner, higher molecular weight macromers lead to more loosely crosslinked, rubbery networks, whereas low molecular weight macromers can be used to synthesize highly crosslinked glassy materials. The chemical nature of the degradable linkage can also alter the degradation rate. For a hydrolytically labile bond, increasing the hydrophobicity around the bond decreases the degradation rate. Furthermore, the degradation mechanism can also be influenced by the network chemistry. Highly hydrophobic networks, as in the poly(anhydrides), tend toward a surface erosion type mechanism [33]. In contrast, degradation in highly swollen hydrogels tends toward a bulk erosion model [32]. The variations available to tune the network properties are quite diverse when one begins to alter the network chemistry and structure through changes in the macromolecular precursor monomers.

The focus of this work is to explore systematic chemical variations in the degradable block of the crosslinked network, while keeping the number of degradable linkages constant. Specifically, macromonomers were synthesized using diethylene glycol (DEG) as an initiator for the ring opening polymerizations of DL-lactide and  $\epsilon$ -caprolactone and combinations of the two monomers (Fig. 1). After functionalization with vinyl moieties, the macromonomers were crosslinked via a photopolymerization process using a visible light initiating system. The tensile moduli, as well as the glass transition temperatures, for the various networks

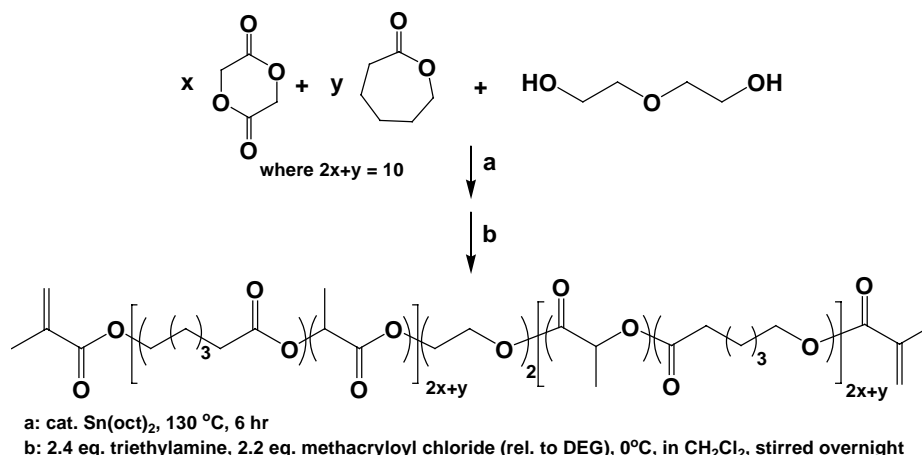


Fig. 1. Synthesis of diethylene glycol/ $\alpha$ -hydroxy acid copolymers containing photopolymerizable end groups.

were recorded. The kinetics of the degradation were followed by measuring the mass loss and compressive modulus changes as a function of time. The implications for using these materials as scaffolds for tissue engineering applications are discussed.

## 2. Experimental

### 2.1. Materials

D,L-Lactide (Polysciences, 100%),  $\epsilon$ -caprolactone (Aldrich, 99%), diethylene glycol (Aldrich, 99%), stannous 2-ethylhexanoate (Sigma, 95%), ethyl 4-dimethylaminobenzoate (DMAB, Aldrich, 99+%) camphorquinone (CQ, Aldrich, 97%) triethylamine (Aldrich, 99.5%) and methacryloyl chloride (Aldrich, 98+%) were used as received without further purification. Solvents were of reagent grade. The phosphate buffer saline solution (PBS) was prepared as a 10X solution (90 g NaCl, 1.72 g  $\text{KH}_2\text{PO}_4$ , 8.15 g  $\text{K}_2\text{HPO}_4$ ) and adjusted to a pH = 7.4.

### 2.2. Methods

#### 2.2.1. Synthesis

**2EG10LA.** D,L-Lactide (LA, 30 g, 0.21 mol) and diethylene glycol (DEG, 2 ml, 0.021 mol) were added to a 250 ml 3-neck round bottom flask equipped with a vacuum adapter on one neck and a stir bar. After covering the open necks with rubber septa, the flask was placed in a 130°C oil bath until the lactide melted. After stannous 2-ethylhexanoate (200  $\mu\text{l}$ ,  $2.2 \times 10^{-4}$  mol) was added, the flask was placed under vacuum and heated for 6 h at 130°C. The flask was cooled, vented to the atmosphere, and the mixture was diluted with methylene chloride (~100 ml). The vacuum adapter was replaced with a sealed addition funnel, and the flask was purged with  $\text{N}_2$  for 30 min. Triethylamine (TEA, 8.8 ml, 63 mmol) was added via a syringe, and the flask was placed on an ice bath. Methylene chloride (50 ml) was added to the addition funnel, followed by methacryloyl chloride (MACl, 5.9 ml, mmol). This solution was added dropwise to the flask over a 2 h period, after which the flask was warmed to room temperature and stirred overnight. Subsequently, the salts were filtered off and the methylene chloride was evaporated. The viscous liquid was redissolved in a minimum amount of benzene and refiltered to remove any remaining salts. This solution was precipitated into a 10-fold excess of cold hexanes (~800 ml), allowed to settle and the hexane was decanted off. The precipitate was redissolved in a minimum amount of methylene chloride and the precipitation cycle was repeated. The remaining solvent was removed by evaporation.  $^1\text{H}$  NMR analysis indicated the presence of 9 lactic acid units/side based on

the ratio of the integrals for the terminal vinyl protons and the LA methyl groups. The methacrylation efficiency was 100% based on the ratio of the integrals for the DEG protons and the terminal vinyl protons.  $^1\text{H}$  NMR ( $\text{CDCl}_3$ ):  $\delta$  = 1.4 (q, methyl group on LA), 1.8 (s, methyl group on terminal vinyl bond), 3.6 (m, ether protons originating from DEG), 4.2 (m, ester protons originating from DEG), 5.0 (m, proton on LA backbone), 5.45 (s, terminal vinyl proton), 6.1 (s, terminal vinyl proton).

**2EG8LA2CL.** LA (12.6 g, 88 mmol),  $\omega$ -caprolactone (CL, 5.1 g, 44 mmol) and DEG (1.2 g, 11 mol) were added to a 250 ml 3-neck round bottom flask equipped with a vacuum adapter on one neck and a stir bar. After covering the open necks with rubber septa, the flask was placed in a 130°C oil bath until the lactide melted. After stannous 2-ethylhexanoate (200  $\mu\text{l}$ ,  $2.2 \times 10^{-4}$  mol) was added, the flask was placed under vacuum and heated for 6 h at 130°C. The flask was cooled, vented to the atmosphere, and the mixture was diluted with methylene chloride (~50 ml). The vacuum adapter was replaced with a sealed addition funnel, and the flask was purged with  $\text{N}_2$  for 30 min. TEA (4.3 ml, 30 mmol) was added via syringe, and the flask was placed on an ice bath. Methylene chloride (50 ml) was added to the addition funnel, followed by MACl (2.7 ml, 27.5 mmol). This solution was added dropwise to the flask over a 2 h period after which the flask was warmed to room temperature and stirred overnight. The work-up was as in I.  $^1\text{H}$  NMR analysis indicated the presence of an average of 7 LA units and 2 CL units/side based on the ratio of the integrals for the DEG backbone protons and the CL/LA backbone protons. The methacrylation efficiency was 83% based on the ratio of the integrals for the DEG protons and the terminal vinyl protons.  $^1\text{H}$  NMR ( $\text{CDCl}_3$ ):  $\delta$  = 1.2–1.6 (m, methyl group on LA and methylene protons on CL), 1.8 (s, methyl group on terminal vinyl bond), 2.3 (m, methylene protons adjacent to carbonyl carbon in CL), 3.6 (m, ether protons originating from DEG), 4.0–4.2 (m, ester protons originating from DEG and adjacent to terminal methacrylate group), 5.0 (m, proton on LA backbone), 5.5 (s, terminal vinyl proton), 6.2 (s, terminal vinyl proton).

**2EG5LA5CL.** The procedure was as for 2EG8LA2CL, but the amounts of reagents added were as follows: LA (7.9 g, 55 mmol), CL (12.5 g, 110 mmol), DEG (1.3 g, 11 mmol), TEA (4.3 ml, 30 mmol), and MACl (2.7 ml, 27.5 mmol).  $^1\text{H}$  NMR analysis indicated the presence of an average of 4 LA units and 5 CL units/side based on the ratio of the integrals for the DEG backbone protons and the CL/LA backbone protons. The methacrylation efficiency was 87% based on the ratio of the integrals for the DEG protons and the terminal vinyl protons.  $^1\text{H}$  NMR ( $\text{CDCl}_3$ ):  $\delta$  = 1.2–1.6 (m, methyl group on LA and methylene protons on CL),

1.8 (s, methyl group on terminal vinyl bond), 2.3 (m, methylene protons adjacent to carbonyl carbon in CL), 3.6 (m, ether protons originating from DEG), 4.0–4.2 (m, ester protons originating from DEG and adjacent to terminal methacrylate group), 5.0 (m, proton on LA backbone), 5.5 (s, terminal vinyl proton), 6.2 (s, terminal vinyl proton).

**2EG2LA8CL.** The procedure was as 2EG8LA2CL, but the amounts of reagents added were as follows: LA (3.2 g, 22 mmol), CL (20.4 g, 176 mmol), DEG (1.1 g, 10 mmol), TEA (4.3 ml, 30 mmol), and MACl (2.7 ml, 27.5 mmol).  $^1\text{H}$  NMR analysis indicated the presence of an average of 2 LA units and 8 CL units/side based on the ratio of the integrals for the DEG backbone protons and the CL/LA backbone protons. The methacrylation efficiency was 100% based on the ratio of the integrals for the DEG protons and the terminal vinyl protons.  $^1\text{H}$  NMR ( $\text{CDCl}_3$ ):  $\delta = 1.2$ – $1.6$  (m, methyl group on LA and methylene protons on CL), 1.8 (s, methyl group on terminal vinyl bond), 2.3 (m, methylene protons adjacent to carbonyl carbon in CL), 3.6 (m, ether protons originating from DEG), 4.0–4.2 (m, ester protons originating from DEG and adjacent to terminal methacrylate group), 5.0 (m, proton on LA backbone), 5.5 (s, terminal vinyl proton), 6.2 (s, terminal vinyl proton).

**2EG10CL.** The procedure was as for 2EG8LA2CL, but the amounts of reagents added were as follows: CL (48.1 g, 422 mmol), DEG (2.2 g, 21 mmol), TEA (8.9 ml, 64 mmol), and MACl (5.2 ml, 53 mmol).  $^1\text{H}$  NMR analysis indicated the presence of an average of 8–9 CL units/side based on the ratio of the integrals for the DEG backbone protons and the CL backbone protons. The methacrylation efficiency was 70% based on the ratio of the integrals for the CL protons and the terminal vinyl protons.  $^1\text{H}$  NMR ( $\text{CDCl}_3$ ):  $\delta = 1.2$ – $1.6$  (m, methylene protons on CL), 1.9 (s, methyl group on terminal vinyl bond), 2.3 (t, methylene protons adjacent to carbonyl carbon in CL), 3.6 (t, ether protons originating from DEG), 4.0–4.2 (m, ester protons originating from DEG and CL), 5.5 (s, terminal vinyl proton), 6.2 (s, terminal vinyl proton).

### 2.2.2. Kinetic experiments

Polymerization rates were measured for 2EG8LA2CL, 2EG5LA5CL, and 2EG2LA8CL. 2EG10LA has been investigated previously [34], and 2EG10CL was eliminated based on the solid nature of the oligomer. 10 wt% CQ (0.500 g) and DMAB (0.504 g) solutions were prepared in ethanol (5.00 g, 5.07 g, respectively). The macromers ( $\sim 0.25$  g each) were added to weigh boats, along with 12.5  $\mu\text{l}$  of each initiator solution, resulting in 0.5 wt% initiator. Approximately 5 mg of sample was weighed into an aluminum DSC pan, which was subsequently placed in the DSC chamber under an  $\text{N}_2$  flow at 25°C after the

light source (EFOS Novacure,  $\lambda = 400$ – $500$  nm,  $I_0 = 160$   $\text{mW}/\text{cm}^2$  at the sample) had been balanced. After allowing the sample to equilibrate thermally ( $\sim 1$  min), the sample was exposed to the initiating light, and the heat flow was monitored as a function of time. The rate of polymerization was calculated based on Eq. (1):

$$R_p = \frac{|Q|}{\Delta H_{\max}} \quad (1)$$

where  $R_p$  is the rate of polymerization in conversion per second,  $Q$  is the heat flow in mW, and  $\Delta H_{\max}$  is the theoretical maximum heat evolved if all the double bonds in the sample are reacted. For these calculations,  $Q$  was corrected by taking the difference between the normalized heat flow and the baseline with the light on and  $\Delta H_{\max}$  was determined from the sample mass multiplied by the  $\Delta H_{\text{rxn}}$ , which is equal to  $\Delta H$  for the methyl ester of methacrylic acid ( $-13.1$  kcal/mol at 25°C) [35] multiplied by the % methacrylation (see Table 2) times 2 double bonds/molecule. The conversion was calculated from the integral of the rate curve over time.

### 2.2.3. Scaffold preparation for degradation and cell seeding experiments (using 2EG10LA as an example)

2EG10LA (1.538 g) was placed in a weigh boat, along with 75  $\mu\text{l}$  of each initiator solution (described in 2), resulting in 0.5 wt% initiator. The solution was mixed to distribute the initiator solution evenly, covered with aluminum foil, then allowed to sit for  $\sim 15$  min to allow the ethanol to evaporate. The solution was then placed between two glass slides held apart with 1 mm spacers, clipped secure, and exposed to visible light at 450 nm (Electro-Lite Corp.) for approximately 10 min on either side. Five millimeter diameter disks were punched out of the resulting polymer sheet. All other polymer networks were prepared in the same manner with the exception of the 2EG10CL, which, because it was a solid, was prepared as a slurry in a minimal amount of acetone to distribute the initiator more effectively. The acetone was evaporated prior to polymerization.

### 2.2.4. Degradation experiments

Preweighed polymer disks ( $D = \sim 5$  mm,  $t = \sim 1$  mm) were placed in histology cassettes and exposed to phosphate buffered saline solution, which was changed every 3–4 days. Triplicate samples were removed every three weeks, subjected to compression testing, and then dried under vacuum to obtain a constant weight. The percent mass loss was calculated from the difference between the initial and final dry weights of the polymer disks, divided by the initial weight.

### 2.2.5. Compression testing

After zeroing and taring the probe, samples were placed between parallel plates, and the heights were measured. A 10 mN force was applied on the sample and increased to 4000 mN at a rate of 100 mN/min. The resulting sample stress (Pa) was measured as a function of the percent strain. The modulus was calculated from the slope of the best fit line of the linear region of the stress-strain curve at less than 10% deformation. Results were obtained in triplicate.

### 2.2.6. Dynamic mechanical testing with temperature

Macromer solutions were prepared as above, but they were polymerized in teflon molds ( $20 \times 5 \times 1$  mm) to produce rectangular strips for use in extension measurements. After taring and zeroing the probe, the samples were clamped between two extension mounts and cooled to  $-60^\circ\text{C}$ . After measuring the probe position, the samples were subjected to sinusoidal forces appropriate to the sample (see Table 1), while the temperature was increased to  $100^\circ\text{C}$  at a rate of  $5^\circ\text{C}/\text{min}$ . The storage moduli were measured as a function of temperature. Dynamic control was applied upon observance of the maximum in the loss-tangent curve (i.e. the glass transition temperature ( $T_g$ )). Experiments were performed in triplicate.

### 2.2.7. Cell seeding experiments

Primary rat calvarial osteoblasts were isolated as described elsewhere [36]. Osteoblasts were cultured in Dulbecco's modified eagle medium (Invitrogen) supplemented with 10% FBS and 1% penicillin/streptomycin (Invitrogen). Polymer disks (10 mm diameter, 1 mm thickness) were sterilized under ultraviolet light. After washing with sterile PBS and prewetting with media, osteoblasts were trypsinized from culture dishes and seeded on the polymer disks at a density of 40,000 cells/cm<sup>2</sup>. After 2 and 6 h, the polymers were rinsed with PBS and fixed with a 2.5% glutaraldehyde solution in a sodium cacodylate buffer (pH 7.4) for 15 min. The polymers were washed with the cacodylate buffer and stained in a 1% osmium tetroxide solution for 45 min at room temperature. After several washes with deionized water, the samples were freeze dried,

sputter coated with gold, and viewed with a scanning electron microscope.

### 2.3. Characterization

<sup>1</sup>H NMR measurements were made on a Varian instrument at 300 MHz using CDCl<sub>3</sub> as a solvent. DSC measurements were made on a Perkin-Elmer Pyris 7 equipped with a subambient cooling apparatus under an inert N<sub>2</sub> atmosphere. Mechanical testing was performed on a Perkin Elmer DMA7e equipped with 10 mm diameter parallel plates or a 5 mm width extension apparatus. Scanning electron micrographs (SEM) were made on an ISI SX30 instrument.

## 3. Results

### 3.1. Macromer synthesis

Crosslinked degradable networks are desirable for a variety of medical applications, including orthopedic fixation devices and controlled drug release systems. The macromers described here will form highly crosslinked networks upon photopolymerization with enhanced mechanical properties compared to hydrogel type materials. The goal of this work was to alter the composition of the macromers systematically while keeping the number of degradable linkages in the crosslinks constant. These compositional variations lead to differences in the macromer molecular weight, and the subsequent concentration of crosslinkable double bonds, so we aimed to investigate the effects of the macromer chemistry on both the mechanical properties as well as on the degradation profiles of the resulting networks.

In a variation of the method first reported by Sawhney et al. [28] diethylene glycol was used as the initiator in the presence of stannous 2-ethylhexanoate as the catalyst for the ring opening polymerizations of mixtures of D,L-lactide and  $\epsilon$ -caprolactone to prepare oligomeric poly( $\alpha$ -hydroxy esters). After methacrylation, the macromers were characterized by <sup>1</sup>H NMR. The experimentally determined compositions agreed well with those predicted by the initial molar ratio of LA:CL in the feed. The percent methacrylation varied from 70–100% (Table 2), which influences the ratio of divinyl to monovinyl macromer in the system. For example, at 70% methacrylation, the macromer mixture will consist of 49% divinyl, 42% monovinyl, and 9% unreactive macromer. Thus, both the size of the macromer and the percent modification of the macromer end groups can be used to control the final concentration of double bonds in the system, which ultimately affects the polymerization behavior and the network structure. Furthermore, unreactive macromer contributes to the overall sol fraction.

Table 1  
Experimental conditions for DMA extension measurements for 2EG-based crosslinked networks

Sample	Forces: static/dynamic (mN)	$w_A, w_B^a$
poly(2EG10LA)	1000/888	1, 0
poly(2EG8LA2CL)	800/666	0.68, 0.32
poly(2EG5LA5CL)	600/500	0.33, 0.67
poly(2EG2LA8CL)	800/666	0.14, 0.86

<sup>a</sup>  $w_A$  = weight fraction of LA,  $w_B$  = weight fraction of CL.

Table 2  
Macromer characteristics

Macromer	Theo. LA:CL (per side)	Exp. LA:CL <sup>a</sup>	Methacrylation efficiency (%) <sup>a</sup>	Molecular weight <sup>a</sup>	Conc. of double bonds <sup>b</sup> (M)
2EG10LA	10:0	9:0	100	1570	1.27
2EG8LA2CL	8:2	7:2	83	1740	0.95
2EG5LA5CL	5:5	4:5	87	1990	0.87
2EG2LA8CL	2:8	2:8	100	2390	0.84
2EG10CL	0:10	0:9	70	2330	0.60

<sup>a</sup> As determined from <sup>1</sup>H NMR analysis.

<sup>b</sup> [(1000 g/l)/(molecular weight g/mol)](2 bonds/macromonomer)(% methacrylation).

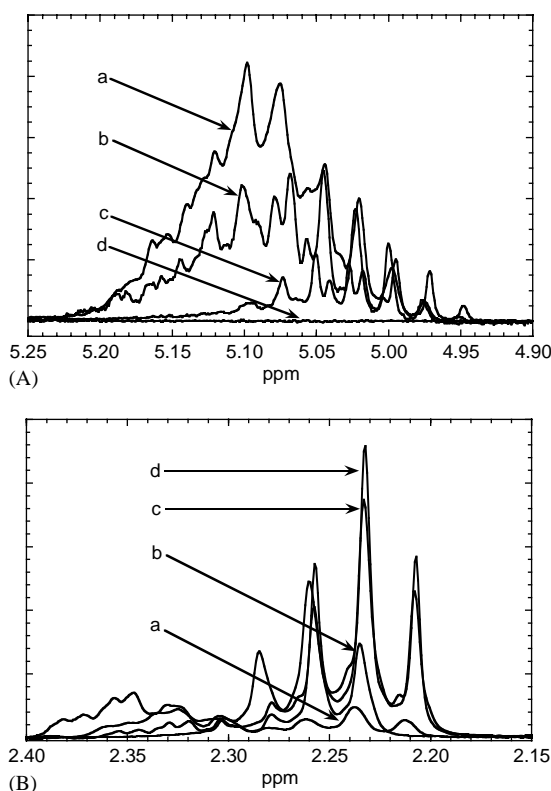


Fig. 2. <sup>1</sup>H NMR spectra (CDCl<sub>3</sub>, 300 MHz) of the lactic acid methylene (A) and caproic acid alkyl (B) regions of 2EG8LA2CL (a), 2EG5LA5CL (b), 2EG2LA8CL (c), and 2EG10CL (d).

Fig. 2A shows the <sup>1</sup>H NMR spectra of the methylene protons present on the lactic acid repeat units, the concentration of which decreases as a function of increasing concentration of caproic acid in the macromer backbone. Concurrently, the alkyl region of the spectra due to caproic acid becomes more intense (Fig. 2B). Changing the composition of the macromer significantly affected the fluid properties. From gross observation, the viscosity of the macromers is as follows: 2EG10CL > 2EG10LA > 2EG8LA2CL ≈ 2EG2LA8CL > 2EG5LA5CL. The 2EG10CL is a solid, while the 2EG5LA5CL is a low viscosity liquid.

### 3.2. Kinetic experiments

The photopolymerizations of 2EG8LA2CL, 2EG5LA5CL, and 2EG2LA8CL were followed by DSC to ascertain the polymerization behavior as a function of time and conversion. The rate of polymerization,  $R_p$  was normalized by the initial concentration of double bonds for each monomer, so differences in the rate profiles were attributed to variations in the kinetics that results from the network structure evolution. As will be demonstrated later, these monomers lead to networks with significantly different crosslinking densities and  $T_g$ s.

Using a visible light responsive initiating system (0.5 wt% CQ/DMAB), the macromonomer solutions were exposed to a 400–500 nm light at an intensity of 160 mW/cm<sup>2</sup> at 25°C, and the change in the heat flow was recorded as a function of exposure time and converted to  $R_p$  as discussed in the experimental section. Fig. 3a plots  $R_p$  vs. time for each of the three oligomers, while Figure 3b details the  $R_p$  vs. conversion. Several characteristic features of multifunctional monomer systems are observed in the rate profiles and include autoacceleration, autodeceleration, and limiting double bond conversions. Furthermore, the maximum rate of polymerization increased in the order 2EG2LA8CL < 2EG5LA5CL < 2EG8LA2CL, which follows an increase in the double bond concentration from 0.84 to 0.87 to 0.95 M, respectively and all polymerizations reached ≥80% double bond conversion within 2 min.

To further analyze these results, applying the pseudo steady state approximation to the radical species, the rate of polymerization is given by  $R_p$ :

$$R_p = k_p[M] \left( \frac{R_i}{2k_t} \right)^{1/2} \quad (2)$$

Here, the polymerization rate is dependent upon the kinetic constant of propagation for the double bond chemistry (e.g., methacrylate),  $k_p$ , the concentration of double bonds,  $M$ , (see Table 2), and the square root of the ratio of the rate of initiation,  $R_i$ , to the termination kinetic constant,  $k_t$ . Assuming that  $R_i$  is the same in each polymerization, the difference in the maximum  $R_p$  for the different oligomers may potentially be attributed

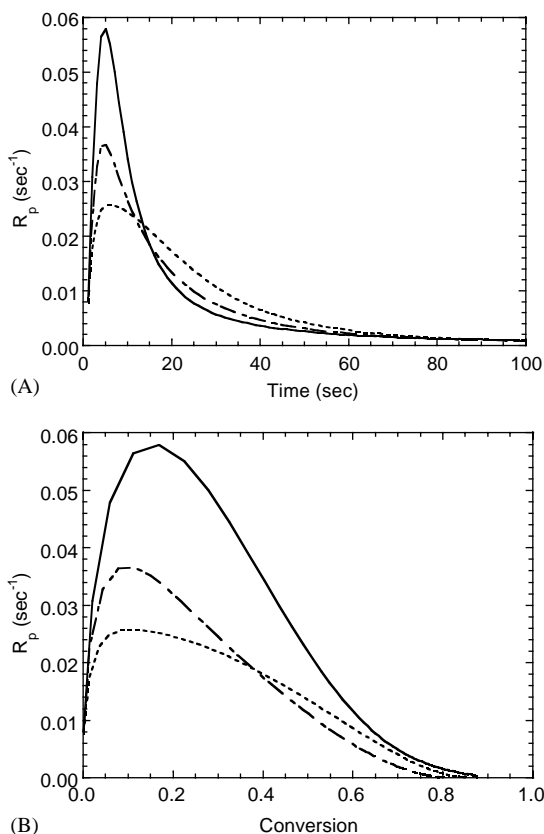


Fig. 3. Plots of (A)  $R_p$  ( $\text{s}^{-1}$ ) vs. Time (s) and (B)  $R_p$  vs. Conversion for 2EG8LA2CL (solid line), 2EG5LA5CL (dashed line) and 2EG2LA8CL (dotted line) as determined from DSC measurements using 0.5 wt% initiator and exposure to 400–500 nm UV light at  $T = 25^\circ\text{C}$ .

to either differences in the  $k_p$ s or to differences in the ratio of  $k_p$  to  $k_t^{1/2}$ . Since the polymerizations were performed at  $25^\circ\text{C}$ , which is slightly below the  $T_g$  of the poly(2EG8LA2CL) network (vide infra),  $k_t$  may become diffusion limited earlier in the reaction, leading to a larger  $R_p$ . In contrast, in the systems that are polymerized above their  $T_g$  (2EG5LA5CL and 2EG2LA8CL), the magnitude of the autoacceleration may not be as large due to a less dramatic decrease in  $k_t$  than observed in the more glassy system. Additionally, the crosslinkable double bond concentration decreases in going from 2EG8LA2CL to 2EG5LA5CL to 2EG2LA8CL, which effectively decreases  $R_p$ . Overall, the photopolymerization behavior of these macromers follows trends established for multifunctional monomer systems and their diffusion controlled kinetics [37].

### 3.3. Degradation profiles

After photopolymerizing the macromers to form crosslinked networks, (5 mm diameter  $\times$  1 mm thick) disks were exposed to PBS solution at  $\text{pH} = 7.4$  and incubated at  $37^\circ\text{C}$  in an orbital shaker. Fig. 4 details the % mass loss as a function of degradation time. The

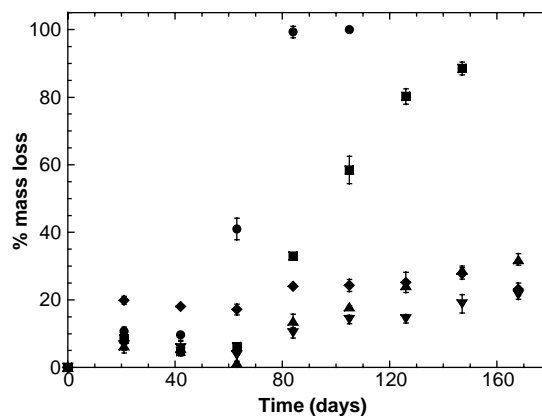


Fig. 4. Plot of % mass loss vs. time for 2EG-based networks of various compositions exposed to PBS ( $\text{pH} = 7.4$ ,  $T = 37^\circ\text{C}$ ): poly(2EG10LA) ( $\bullet$ ), poly(2EG8LA2CL) ( $\blacksquare$ ), poly(2EG5LA5CL) ( $\blacktriangle$ ), poly(2EG2LA8CL) ( $\blacktriangledown$ ), poly(2EG10CL) ( $\blacklozenge$ ).

poly(2EG10LA) network completely degraded by 105 days ( $\bullet$ ), followed shortly thereafter by the poly(2EG8LA2CL) network, which lost  $\sim 90\%$  mass after 147 days ( $\blacksquare$ ). However, the remaining networks appeared to be losing mass at a much slower rate with only 20–30% mass loss after 164 days. Swelling studies performed in methylene chloride indicated that the initial mass loss ( $< 20\%$ ) observed in those samples that did not degrade within the time frame of the experiment (i.e., 164 days) may be attributable to the presence of a small sol fraction.

In these networks, the mass loss is a function of both the hydrolysis kinetics and the network structure. For example, the degradable blocks on both sides of the DEG core must cleave before the crosslink can diffuse from the network, while the majority of the degradable linkages must hydrolyze before the kinetic chains are released. Furthermore, diffusion of the eroded products from the network is a function of the network crosslinking density, which also changes with degradation. Thus, in highly crosslinked, yet relatively hydrophilic systems, one might expect the mass loss profile to have an induction period while the labile bonds are hydrolyzed, followed by a significant increase in the % mass loss as degradation products are released, which is the case for the poly(2EG10LA) and poly(2EG8LA2CL) networks. However, although the mesh size of the poly(2EG8LA2CL) network is larger than that of the poly(2EG10LA), resulting from the increase in the macromer molecular weight (Table 2), the erosion rate is slower. This trend continues as the content of CL in the network increases, which indicates that the faster erosion rate usually associated with an increase in the mesh size is offset by the increasing hydrophobicity as the composition of CL in the network increases. These results nicely demonstrate the significant effects that the lability of the degradable linkage can have on network properties.

### 3.4. Mechanical properties

Samples of the various networks were subjected to dynamic mechanical analysis in extension mode to determine the network glass transition temperatures ( $T_g$ ) as a function of the temperature (Fig. 5). The static and dynamic stresses applied to the networks varied (Table 1). The  $T_g$  was taken from the maximum in the loss tangent curve ( $\tan \delta$ ). As expected, the  $T_g$  decreased as the content of CL in the network increased due to an increased mobility in the crosslinks resulting from the long CL alkyl chain. These values were in relatively good agreement with those predicted by Eq. (3),

$$T_{gco} = T_{gA}^{w_A} + T_{gB}^{w_B} \quad (3)$$

which defines the  $T_g$  of a copolymer to be dependent upon the  $T_{gs}$  of the individual components and the weight fraction of those components,  $w$ , in the copolymer (see Table 1). The  $T_g$  of the LA segment was taken as 55°C and that of the CL segment, -60°C [38].

Control over the  $T_g$  is advantageous for biomaterials applications since this property can heavily influence the suitability of a material for a given application. In general, these crosslinked polymers displayed relatively broad transitions from the glassy to rubbery plateaus, spanning several decades of temperature. In Fig. 6, the initial moduli of the networks were comparable when all were in the glassy state and around  $5 \times 10^8$  Pa. The onset of the transition to the rubbery state followed the same trend as the  $T_{gs}$  of the various networks; the lowest onset was observed for the poly(2EG2LA8CL) while the highest was for the poly(2EG10LA). The broad transitions ( $\sim 35$ – $40^\circ\text{C}$ ) indicate heterogeneity in the systems, as expected for such highly crosslinked systems where mobility is limited. While the poly(2EG10LA) and poly(2EG8LA2CL) samples all broke prior to reaching the ultimate rubbery plateau, the

poly(2EG5LA5CL) approached a rubbery plateau approximately 2 orders of magnitude below its glassy state modulus. Because the modulus in the rubbery plateau is proportional to the number of elastically active crosslinks in the network [39], these results suggest that there are differences in the crosslinking densities in these systems: poly(2EG10LA) > poly(2EG8LA2CL)  $\sim$  poly(2EG5LA5CL) > poly(2EG2LA8CL). This trend also corresponds to the concentration of double bonds in the various macromers (Table 2). The poly(2EG2LA8CL) also showed what appeared to be a melt transition at 60–80°C, in relative agreement with published values [40], followed by a rubbery plateau similar in magnitude to the other networks. Since crystalline regions are unusual in densely crosslinked networks, these results are quite interesting and suggest that the backbone possesses a somewhat blocky structure rather than randomly placed CL segments and sufficient mobility in the network crosslinks to enable crystallization prior to or post-polymerization.

Each sample used in the degradation study was subjected to compression testing to determine the effect of degradation on the network structure. Fig. 7 is a plot of the log(Compressive Modulus) vs. Time for poly(2EG10LA) and poly(2EG8LA2CL) exposed to PBS buffer at 37°C. From rubbery elasticity theory, the compressive modulus is proportional to the number of crosslinks in the network; however, the crosslinks are hydrolyzed with time. For a simple case of pseudo first order hydrolysis of the degradable segments (i.e., for a homogeneous bulk degradation process), the number of crosslinks will exponentially decay with time and will be reflected in the semi-log plot of the compressive modulus [32]. The linear relationship between the compressive modulus and time indicates that the poly(2EG10LA) follows a bulk degradation mechanism (Fig. 7, (●)). In contrast, the compressive modulus did not change considerably for the poly(2EG8LA2CL) network until

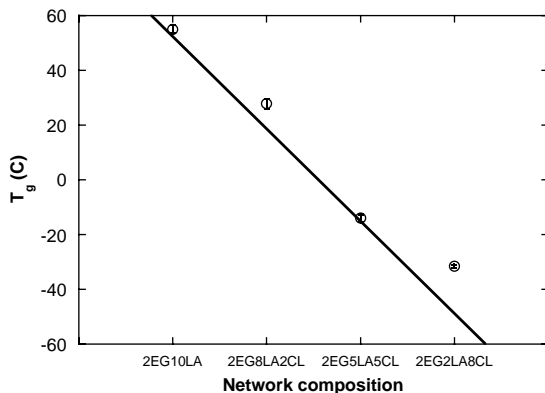


Fig. 5. Plot of the Glass transition temperature ( $T_g$ ) vs. Network composition for 2EG-based degradable networks prepared via a photopolymerization process; (O): experimental results, (—): theoretical results predicted by Eq. (3).

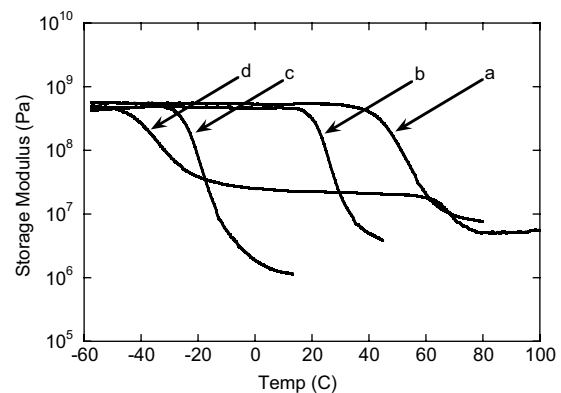


Fig. 6. Plot of Storage Modulus vs. Temperature for poly(2EG10LA) (a), poly(2EG8LA2CL) (b), poly(2EG5LA5CL) (c), and poly(2EG2LA8CL) (d) crosslinked networks. Experimental conditions detailed in Table 1.

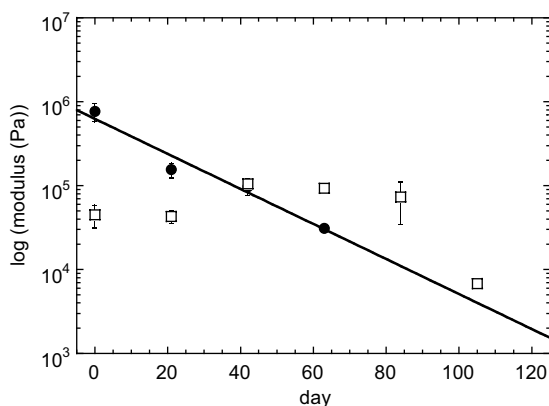


Fig. 7. Plot of  $\log(\text{compressive modulus})$  vs. degradation time for poly(2EG10LA) (■) and poly(8LA2CL) (□).

> 40% total mass loss (Fig. 4 (■) and 7(□)). While the mass loss profile indicated that degradation occurred via a bulk erosion mechanism, the compression testing results suggest a combination of both a bulk and surface eroding mechanism. An additional point is that the initial compressive modulus for the poly(2EG8LA2CL) network was an order of magnitude lower than that of the poly(2EG10LA) network. The compressive moduli of the remaining networks (poly(2EG5LA5CL), poly(2EG2CL8LA), and poly(2EG10CL)) showed no change with time, as expected since hydrolysis of the labile esters was assumed to be minimal. The moduli ranged from  $10^5$  to  $10^6$  Pa.

### 3.5. Cell seeding experiments

Primary rat calvarial osteoblasts were seeded on polymer scaffolds of varying composition, and their morphology was assessed using scanning electron microscopy (SEM) after incubation at  $37^\circ\text{C}$  for various time periods. Figs. 8a and c show cells seeded on poly(2EG10LA) scaffolds after 2 and 6 h, respectively, while Fig. 8b and d show the cells seeded on the poly(2EG10CL) network, again after 2 and 6 h, respectively. On both scaffolds the cells adhered and spread on the surface and were confluent after a minimal incubation period due to the high seeding density. These examples were chosen as the extremes of the types of scaffolds investigated in terms of both degradation time and hydrophobicity. Cells seeded on the other network compositions behaved similarly. That the cells did not necessarily distinguish between the different networks is not unexpected since the hydrophobicity increased as the content of CL in the network increased; protein adsorption to surfaces is generally enhanced as the hydrophobicity increases, which encourages cellular adhesion and spreading. This bodes well for tissue engineering applications since this suggests that simple changes in macromer chemistry may lead to crosslinked

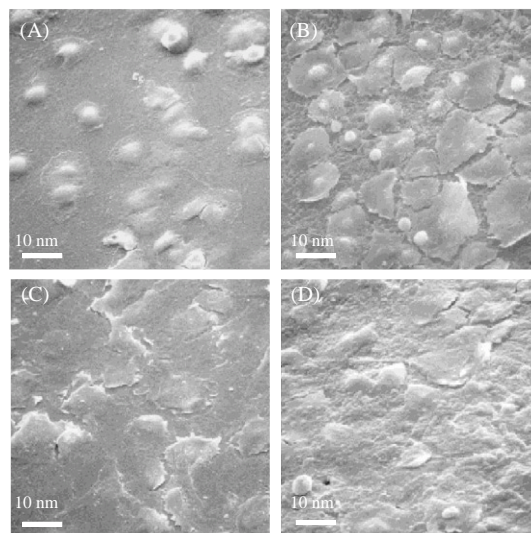


Fig. 8. SEM images of primary rat calvarial osteoblasts seeded on photopolymerized scaffolds of poly(2EG10LA) after 2 (A) and 6 h (C) and on poly(2EG10CL) after 2 (B) and 6 h (D); bar = 10 nm.

degradable networks with a range of physical, mechanical, and chemical properties, while maintaining and promoting cell attachment and function (Fig. 8).

## 4. Discussion

The materials described here exhibited very different properties as a result of small changes in the overall chemistry of the macromers used to form the degradable crosslinked networks. The addition of even small amounts of caproic acid into the macromer backbone increased the degradation time of the crosslinked scaffolds significantly from those composed solely from lactic acid-based macromers; the time to complete degradation can be tuned by choosing the proper ratio between the two components. The presence of the longer alkyl chain in the CL compared with the LA also produced higher modulus matrices but with lower  $T_g$ s, which may be advantageous for applications where increased elasticity is important. While the compressive moduli varied as a function of the composition, the storage moduli in the glassy regime were of the same order of magnitude for all the networks. After the transition to the rubbery plateau, however, the differences in the moduli suggested that the crosslinking densities varied among the networks, which correlated with the concentration of crosslinkable double bonds in the systems.

Cell attachment was not significantly affected by the changes in the network composition, suggesting the possibility of a material platform that can support cell attachment and function, but be easily modified to possess varying degradation profiles and/or mechanical

properties. Finally, the use of photoinitiated polymerizations offers spatial and temporal control not easily achieved with other polymerization approaches. The success of using a visible light initiating system to prepare the crosslinked degradable networks makes these biomaterials an ideal candidate for in vivo applications

## 5. Conclusions

Photopolymerized highly crosslinked degradable networks were prepared from dimethacrylated macromers containing lactic and caproic acid segments. The polymerization rate decreased as a function of increasing caproic acid content, which was most likely due to the combined effects of the decrease in double bond concentration with increasing macromer molecular weights and increased chain mobility in the less glassy systems. The glass transition temperatures of the networks decreased as the content of caproic acid in the macromer increased and agreed well with theoretical values predicted from the compositions determined from  $^1\text{H}$  NMR analysis. The storage moduli were on the order of  $10^9$  Pa for the poly(2EG10LA), the poly(2EG8LA2CL), the poly(2EG5LA5CL) and the poly(2EG2LA8CL) networks in the glassy regime and based on the modulus in the rubbery regime, slight variations in the network structures were inferred. An additional melt transition was observed in the poly(2EG2LA8CL) network.

The rate of mass loss in the degradable systems decreased as the network hydrophobicity increased; the poly(2EG10LA) networks degraded fully in just over 80 days, while the poly(2EG8LA2CL) networks lost > 90% mass after 145 days. Networks composed of > 50% caproic acid showed minimal mass loss after 6 months. The compressive moduli of the poly(2EG10LA) networks decreased linearly as a function of degradation time, in agreement with a bulk eroding mechanism depicted by the mass loss profile. In contrast, while the mass loss profile of the poly(2EG8LA2CL) network also supported a bulk erosion mechanism, the compressive moduli did not decrease significantly until greater than 50% mass loss, suggesting degradation occurred via a combination of bulk and surface eroding mechanisms. The compressive moduli of the networks composed of > 50% caproic acid did not change significantly over the course of the degradation experiment, as expected from the minimal mass loss profiles.

Primary rat calvarial osteoblasts cells seeded on scaffolds prepared from poly(2EG10LA) and poly(2EG10CL) were spread on the surface after 2 h and formed a confluent cell layer after 6 h. Similar results were obtained with the scaffolds prepared from the intermediate composition macromers, suggesting

these highly crosslinked degradable scaffolds are cellularly compatible and promote osteoblast attachment.

## Acknowledgements

The authors wish to acknowledge funding from an NIH research grant (AR44375-02) as well as from HHMI for a postdoctoral fellowship to KAD and the NSF and GAANN Foundation for graduate fellowships to JAB.

## References

- [1] Yaszemski MJ, Payne RG, Hayes WC, Langer RS, Aufdemorte TB, Mikos AG. The ingrowth of new bone tissue and initial mechanical properties of a degrading polymeric composite scaffold. *Tissue Eng* 1995;1:41–52.
- [2] Suggs LJ, Payne RG, Yaszemski MJ, Alemany LB, Mikos AG. Synthesis and characterization of a block copolymer consisting of poly(propylene fumarate) and poly(ethylene glycol). *Macromolecules* 1997;30:4318–23.
- [3] Muggli DS, Burkoth AK, Keyser SA, Lee HR, Anseth KS. Reaction behavior of biodegradable, photo-cross-linkable polyanhydrides. *Macromolecules* 1998;31:4120–5.
- [4] Anseth KS, Shastri VR, Langer R. Photopolymerizable degradable polyanhydrides with osteocompatibility. *Natl Biotechnol* 1999;17:156–9.
- [5] Young JS, Gonzales KD, Anseth KS. Photopolymers in orthopedics: characterization of novel crosslinked polyanhydrides. *Biomaterials* 2000;21:1181–8.
- [6] He S, Yaszemski MJ, Yasko AJ, Engel PS, Mikos AG. Injectable biodegradable polymer composites based on poly(propylene fumarate) crosslinked with poly(ethylene glycol)-dimethacrylate. *Biomaterials* 2000;21:2389–94.
- [7] Burkoth AK, Anseth KS. A review of photocrosslinked polyanhydrides: in situ forming degradable networks. *Biomaterials* 2000;21:2395–404.
- [8] Burdick JA, Davis KA, Anseth KS. Synthesis and application of multifunctional lactide and caprolactone based oligomers for orthopaedic tissue engineering. *Polym Mater Sci Eng* 2001;85: 57–8.
- [9] Metters AT, Anseth KS, Bowman CN. Fundamental studies of biodegradable hydrogels as cartilage replacement materials. *Biomed Sci Instrum* 1999;35:33–8.
- [10] Bryant SJ, Nuttelman CR, Anseth KS. The effects of crosslinking density on cartilage formation in photocrosslinkable hydrogels. *Biomed Sci Instrum* 1999;35:309–14.
- [11] Bryant SJ, Anseth KS. The effects of scaffold thickness on tissue engineered cartilage in photocrosslinked poly(ethylene oxide) hydrogels. *Biomaterials* 2001;22:619–26.
- [12] Bryant SJ, Anseth KS. Hydrogel properties influence ECM production by chondrocytes photoencapsulated in poly(ethylene glycol) hydrogels. *J Biomed Mater Res* 2002;59:63–72.
- [13] Heller J, Fritzing BK, Ng SY, Penhale DWH. In vitro and in vivo release of levonorgestrel from poly(ortho esters). II. Cross-linked polymers. *J Controlled Release* 1985;1:233–8.
- [14] Kurisawa M, Terano M, Yui N. Double-stimuli-responsive degradable hydrogels for drug delivery: interpenetrating polymer networks composed of oligopeptide-terminated poly(ethylene glycol) and dextran. *Macromol Rapid Commun* 1995;16:663–6.

- [15] Kurisawa M, Yui N. Double stimuli-responsive degradable hydrogels: interpenetrating polymer networks of oligopeptide-terminated poly(ethylene glycol) and dextran. *Proc Int Symp Controlled Release Bioact Mater* 1996;23:765–6.
- [16] Hill-West JL, Dunn RC, Hubbell JA. Local release of fibrinolytic agents for adhesion prevention. *J Surg Res* 1995;59:759–63.
- [17] Hubbell JA. Hydrogel systems for barriers and local drug delivery in the control of wound healing. *J Controlled Release* 1996;39:305–13.
- [18] Hennink WE, Franssen O, van Dijk-Wolthuis WNE, Talsma H. Dextran hydrogels for the controlled release of proteins. *J Controlled Release* 1997;48:107–14.
- [19] Stenekes RJH, Loebis AE, Fernandes CM, Crommelin DJA, Hennink WE. Controlled release of liposomes from biodegradable dextran microspheres: a novel delivery concept. *Pharm Res* 2000;17:690–5.
- [20] Stenekes RJH, Loebis AE, Fernandes CM, Crommelin DJA, Hennink WE. Degradable dextran microspheres for the controlled release of liposomes. *Int J Pharm* 2001;214:17–20.
- [21] Elisseeff J, Anseth K, Sims D, McIntosh W, Randolph M, Yaremchuk M, Langer R. Transdermal photopolymerization of poly(ethylene oxide)-based injectable hydrogels for tissue-engineered cartilage. *Plast Reconstr Sur* 1999;104:1014–22.
- [22] Elisseeff J, Anseth K, Sims D, McIntosh W, Randolph M, Langer R. Transdermal photopolymerization for minimally invasive implantation. *Proc Nat Acad Sci, USA*, 1999. vol. 96. p. 3104–7.
- [23] Anseth KS, Newman S, Bowman CN. Polymeric dental composites: properties and reaction behavior of multi-methacrylate dental restorations. *Adv Polym Sci* 1995;122:177–217.
- [24] Bryant SJ, Nuttelman CR, Anseth KS. Cytocompatibility of UV and visible light photoinitiating systems on cultured NIH/3T3 fibroblasts in vitro. *J Biomat Sci* 2000;11:439–57.
- [25] Burdick JA, Anseth KS. Photoencapsulation of osteoblasts in injectable RGD-modified PEG hydrogels for bone tissue engineering applications. *Biomaterials* 2002;23:4315–23.
- [26] Burdick JA, Padera RF, Huang JV, Anseth KS. An investigation of the cytotoxicity and histocompatibility of in situ forming lactic acid based orthopedic biomaterials. *J Biomed Mater Res, Appl Biomater* 2002;63:484–91.
- [27] Davis KA, Anseth KS. Controlled release from crosslinked degradable scaffolds. *Crit Rev Ther Drug Carr Sys*, in press.
- [28] Sawhney AS, Pathak CP, Hubbell JA. Bioerodible hydrogels based on photopolymerized poly(ethylene glycol)-co-poly( $\alpha$ -hydroxy acid) diacrylate macromers. *Macromolecules* 1993;26:581–7.
- [29] van Dijk-Wolthuis WNE, Frassen O, Talsma H, van Steenberghe MJ, Kettenes-van den Bosch JJ, Hennink WE. Synthesis, characterization, and polymerization of glycidyl methacrylate derivatized dextran. *Macromolecules* 1995;28:6317–22.
- [30] Anseth KS, Quick DJ. Polymerizations of multifunctional anhydride monomers to form highly crosslinked degradable networks. *Macromol Rapid Commun* 2001;22:564–72.
- [31] Metters AT, Anseth KS, Bowman CN. Fundamental studies of a novel, biodegradable PEG-*b*-PLA hydrogel. *Polymer* 2000;41:3993–4004.
- [32] Metters AT, Bowman CN, Anseth KS. A statistical model for the bulk degradation of PLA-*b*-PEG-*b*-PLA hydrogel networks. *J Phys Chem B* 2000;104:7043–9.
- [33] Burkoth AK, Burdick J, Anseth KS. Surface and bulk modifications to photocrosslinked polyanhydrides to control degradation behavior. *J Biomed Mater Res* 2000;51:352–9.
- [34] Burdick JA, Philpott LM, Anseth KS. Synthesis and characterization of tetrafunctional lactic acid oligomers: a potential in situ forming degradable orthopaedic biomaterial. *J Polym Sci, Part A: Polym Chem* 2001;39:683–92.
- [35] Leonard J. Heats and entropies of polymerization, ceiling temperatures, equilibrium monomer concentrations, and polymerizability of heterocyclic compounds. In: Brandup J, Immergut EH, Grulke EA, editors. *Polymer handbook*. New York: John Wiley & Sons, Inc., 1999. p. II369.
- [36] Ishaug SL, Yaszemski MJ, Bizios R, Mikos AG. Osteoblast function on synthetic biodegradable polymers. *J Biomed Mater Res* 1994;28:1445–53.
- [37] Lovell LG, Berchtold KA, Elliott JE, Lu H, Bowman CN. Understanding the kinetics and network formation of dimethacrylate dental resins. *Polym Adv Technol* 2001;12:335–45.
- [38] Andrew RJ, Grulke EA. Glass transition temperatures of polymers. In: Brandup J, Immergut EH, Grulke EA, editors. *Polymer handbook*. New York: John Wiley & Sons, Inc., 1999. p. VI222.
- [39] Sperling LH. *Introduction to physical polymer science*. New York: Wiley Interscience, 1992.
- [40] Miller RL. Crystallographic data and melting points for various polymers. In: Brandup J, Immergut EH, Grulke EA, editors. *Polymer handbook*. New York: John Wiley & Sons, Inc., 1999. p. VI44–5.